J Seismol (2019) 23:59–76
https://doi.org/10.1007/s10950-018-9793-2

ORIGINAL ARTICLE

Discrimination of quarry blasts from tectonic events in the Armutlu Peninsula, Turkey

Evrim Yavuz · Fadime Sertçelik · Hamdullah Livaoğlu · Heiko Woith · Birger-Gottfried Lühr

Received: 24 April 2017 / Accepted: 11 September 2018 / Published online: 21 September 2018

Abstract Different methods to discriminate between quarry blasts and earthquakes in seismic records are applied and compared. Test area is the Armutlu Peninsula in northwestern Turkey, where microearthquakes and quarry blasts occur within the same area. The vertical component of a 360″ broadband sensor is used for the discrimination analyses. Eighty-seven seismic events with up to M = 3.0 duration magnitude and maximum 23-km epicentral distance are chosen from the first 7 months of 2014. Five different methods, (1) time distribution, (2) amplitude peak ratio (A_s/A_p–log(A_s)), (3) complexity-spectral ratio (C–Sr), (4) coda wave decay rate (Q_c), (5) power spectrum density (PSD), and two statistical approaches, linear discriminant function (LDF), quadratic discriminant function (QDF), are performed through all seismic events. The results are then compared to a "gold standard" obtained by a careful manual investigation. Two functions are obtained for A_s/A_p–log(A_s) method and four functions with different distances (0–13 km, 13–23 km) are estimated for C–Sr method. Accuracies of LDF and QDF for A_s/A_p–log(A_s) method are 88.5% and 87.4%, respectively. For C–Sr method, an accuracy of 89.8% is obtained for both, LDF and QDF, for distances up to 13 km, whereas for the distance range between 13 and 23 km from the epicenter, the accuracies are 85.7% and 89.3% for LDF and QDF, respectively. According to the Q_c, the success rate is calculated as 91.9%. 93.1% accuracy of PSD technique provides the most successful results. All methods were used for a final decision according to which 27 earthquakes and 55 quarry blasts could be identified, while five events are misclassified. Overall, a 94.2% success rate could be obtained for our test data set. For the Armutlu Peninsula, the PSD method proves to give reliable solutions. Nevertheless, this cannot be generalized and thus a combination of different methods is recommended for areas with high tectonic and mining activity.

Keywords Quarry blast discrimination · Statistical approaches · Time and frequency domain methods · Armutlu Peninsula, Turkey

E. Yavuz · F. Sertçelik (✉) · H. Livaoğlu
Department of Geophysical Engineering, Kocaeli University, Umuttepe, 41380 Kocaeli, Turkey
e-mail: fasert@kocaeli.edu.tr

H. Woith · B.-G. Lühr
GFZ, German Research Centre for Geosciences, Telegrafenberg, 14473 Potsdam, Germany

1 Introduction

The Armutlu Peninsula is located in the Marmara region, between the northern and middle branches of the North Anatolian Fault Zone (NAFZ), which is one of the most active fault zones in Turkey. The region contains many quarries and active mines, where explosives such as dynamite are prevalently used in order to obtain material easily and economically. The explosives cause artificial vibrations and are clearly recorded at seismic stations of the Armutlu network, which is established to record and analyze earthquakes at even micro-scale. It is

very important to detect artificial signals in seismic records and to distinguish them from earthquake events. Many different methods have been proposed to distinguish quarry blasts from tectonic events in seismic records related to parameters as depth of an event, P wave first motion, P and S wave amplitude peak ratio, complexity versus spectral ratio, coda wave decay rate, power spectrum density, Pg/Lg magnitude ratio, and Pn/Sn amplitude ratio (Wüster 1993; Gitterman et al. 1998; Wiemer and Baer 2000; Koch and Fäh 2002; Horasan et al. 2009; Ursino et al. 2001; Yılmaz et al. 2013; Carr and Garbin 1998; Arrowsmith et al. 2006).

Su et al. (1991) performed the discrimination of quarry/mining blasts and earthquakes by using coda wave power spectrum in the area encompassing the south-central Mojave Desert and eastern Transverse Ranges. In 30-s lapse time, especially at low frequencies (1.5–3 Hz), they found higher Q_c^{-1} values for blasts as compared to the earthquakes. It was expressed that this property is not very significant at lapse times of more than 20 s and high frequencies (6–12 Hz). Borleanu et al. (2016) stated in a study they performed for Romania that clearer results could be obtained with the Vp/Vs ratio method with different statistical approaches. Kim et al. (1997) applied the Pg/Lg magnitude ratio technique in southern Russia. While the failure of discrimination was 7% at a 10–20-Hz frequency interval, it was emphasized that Pg/Lg ratios show poor results at a 2–10-Hz interval. Kekovalı et al. (2012) performed a study in western Turkey mining areas, and determined that 344 out of 520 seismic records originated from artificial explosions, by using S/P wave amplitude peak ratio, complexity, and spectral ratio methods. Ataeva et al. (2017) analyzed and compared the P and S wave displacement spectra from local earthquakes and blasts of similar magnitudes. They obtained ratios of P to S wave corner frequencies of 1.23 and 1.86 for earthquakes and explosions, respectively. Shashidhar et al. (2014) examined the seismic events in Koyna-Warna Region. They have checked the temporal and spatial distribution of events and also evaluated waveform data. The surface waves have low energy around 9 Hz. Uniform P wave polarities are the characteristic properties that have been used for a certain discrimination of blasts from earthquakes. Kuyuk et al. (2011) distinguished microearthquakes from quarry blasts in Istanbul, Turkey. Amplitude peak ratio and complexity methods were both applied with unsupervised learning algorithms for event classification. Yıldırım et al. (2011) discriminated the seismic events using software algorithms that feedforward neural networks, adaptive neural fuzzy inference systems, and probabilistic neural networks.

In our study area, where seismic activity and mining areas are prevalent, there has been no study on the separation of natural earthquake activity from artificial sources. We aim to discriminate earthquakes and quarry blasts in the Armutlu Peninsula focusing on the parameters P and S wave amplitude peak ratio, complexity versus spectral ratio, coda wave decay rate, and power spectrum density methods. A combination and comparison of different methods are applied to increase the reliability of the results. Besides that, statistical approaches with linear and quadratic discriminant functions are performed for the event classification. We believe that this study may be helpful for declustering the earthquake catalogs and it should also contribute to seismological studies by providing information on the source type-frequency content relationship of the seismic events.

2 Geological and tectonic structure of the Armutlu Peninsula

Upper Cretaceous-Pliocene sediments cover the northern part of the Armutlu Peninsula. Generally, the western and southwestern parts of the peninsula are characterized by Upper Jurassic-Lower Cretaceous metamorphic rocks and Tertiary granite. Upper Triassic-Middle Jurassic limestones can be widely observed on the southeastern part of the peninsula (Akartuna 1968; Göncüoğlu et al. 1992).

Two main strike-slip fault systems are located in Turkey called NAFZ, which is dextral, and East Anatolian Fault Zone (EAFZ) that is sinistral. The Armutlu Peninsula is positioned at the western part of NAFZ located between the northern and middle strand of this main fault (see in Fig. 1). This main fault zone and its branches are seismically active as revealed by the approximately 24 ± 1 mm/year movement obtained from GPS data (Reilinger et al. 1997, 2006; McClusky et al. 2003).

The region is tectonically complex and produces a large number of microseismic events. The 1999 Kocaeli earthquake occurred along the northern branch of NAFZ and stopped north of the peninsula (see in Fig. 1). Within the study area, no big earthquake has been occurred in

the last century along the middle strand. The Armutlu Peninsula is located close to important cities such as Istanbul, Bursa, and Kocaeli and its active tectonics have been investigated by many researchers and institutions (Eisenlohr 1997; Armijo et al. 1999; Robertson and Ustaömer 2004; Tunç et al. 2011; Kinscher et al. 2013).

In the Armutlu Peninsula, the seismic activity is a mix of tectonic events, quarry blasts (mostly in limestone areas), and events related to geothermal sources. For example, in 2014, fi a seismic swarm occurred at the geothermal reservoir of Termal (Yavuz et al. 2015).

3 Data set

Station KRSK is one of the seismic stations of the ARmutlu NETwork (ARNET) that is operated by Kocaeli University Earth and Space Sciences Research Center (ESSRC) and GFZ German Research Centre for Geosciences. In this study, KRSK recordings were used to discriminate earthquakes and quarry blasts at different explosion sites as this station has recorded events more clearly than others. It has a 360″ broadband sensor (GÜRALP) and at sampling rate set to 100 samples per second. Only the vertical component of the seismograms was used for calculation. One hundred seven events were cataloged for the first 7 months of the year 2014; however, some of them were compulsorily eliminated due to some technical problems (power loss, non-recording signals, etc.) of station KRSK. Eighty-seven seismic events with high signal/noise ratio records were chosen (Fig. 1).

Within each quarry, explosions took place less than a few hundred meters apart from each other and their energy release is not as high as that of earthquakes.

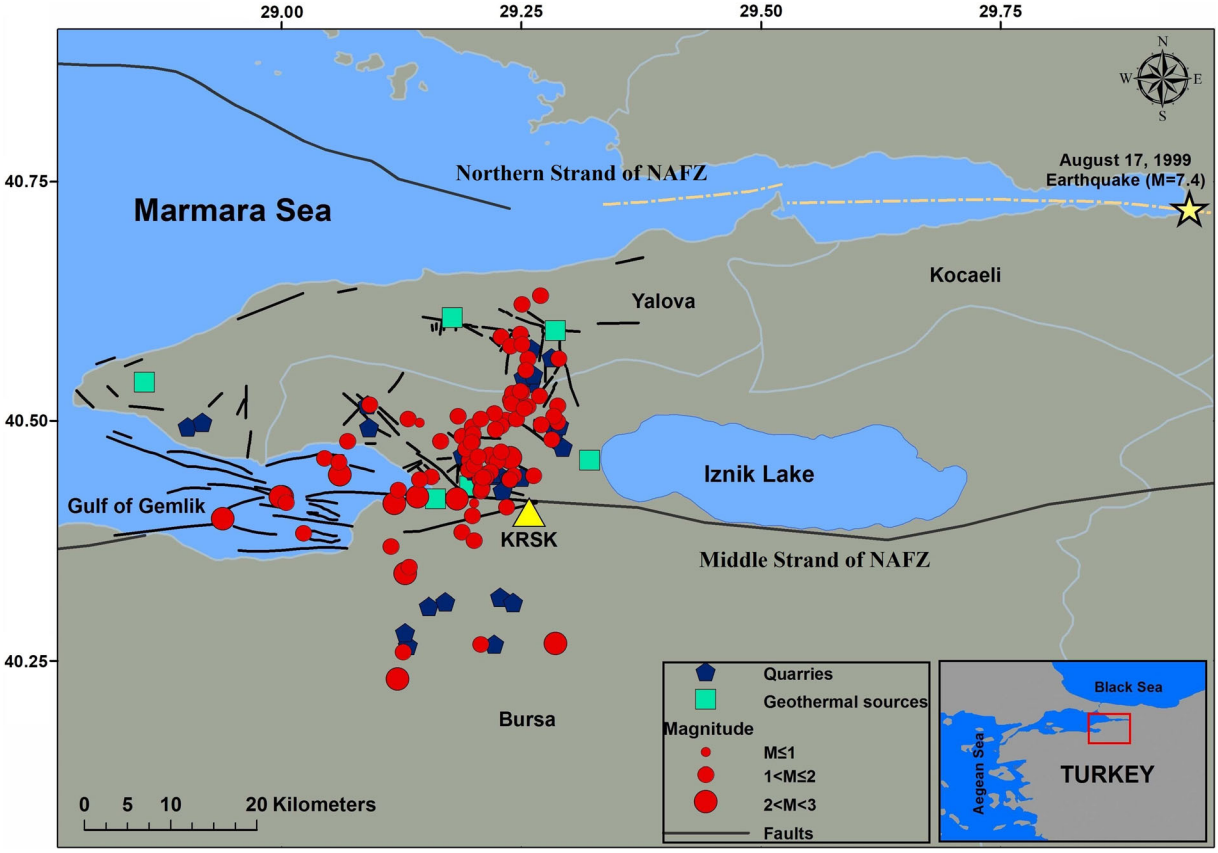

Fig. 1 Location of "seismic" events (red circles) in the first 7 months of 2014 in and around the Armutlu Peninsula. The seismic station KRSK is the yellow triangle. Green squares show the geothermal sources (Eisenlohr 1997), and blue pentagons depict quarries. The black lines indicate the North Anatolian Fault Zone as well as other faults (Kuşçu et al. 2009; Çaka 2012). The yellow star shows the epicenter of the August 19, 1999, Kocaeli Earthquake (M = 7.4) and the dashed yellow line marks the western rupture of this earthquake (Barka et al. 2002)

However, regarding the sensitivity of depth solutions, it is useful to increase the depth limit (Aki and Richards 1980; Sertçelik and Başer 2010). Maximum 10 km of focal depth, 0 to 23 km of epicentral distance, and up to $M_d = 3.0$ duration magnitudes were selected for discriminant analyses.

SEISAN software (Havskov and Ottemoller 1999) was used to determine the location of the events. To improve the location quality, minimum five stations' records for each event which are azimuthally distributed were taken into account.

With respect to the waveforms of events—due to the different source mechanisms—P wave peak amplitudes are much higher than other phases in signals from quarry blast explosions (point source); otherwise, earthquakes (plane source) have higher amplitudes of S and surface waves. When the distance between epicenter and station increases, the seismograms often begin to alter from this general view. Thus, a more detailed investigation of seismograms was needed. In this context, five different methods and two statistical approaches were used to discriminate the quarry blasts from tectonic events.

4 Methodologies and results

In this study, five different techniques that are both in time and frequency domain were applied to the station KRSK recordings of the 87 events with epicenters in the vicinity of the explosion sites.

The signals were first evaluated manually taking into account the following criteria: P wave first motion, no S wave recording, high amplitude of P wave, Rg phase appearance, shallow depth, daytime of occurrence, and distance to quarries. This manual identification is named as "gold standard" and was used to calculate the accuracy of the other techniques (Table 2 in the Appendix).

4.1 Daytime of event

The quantity of explosions increases during day time which corresponds to regular blasting hours of the quarries. To identify preferred blasting times, UTC has been converted to local summer and winter time. In case an "event" occurred before 11:00 and after 19:00 local time, the respective event source was marked as "EQ" (Table 2 in the Appendix). Each day, the average "seismic" activity increases with a sharp onset at 11:00 local time. Increasing day time activity is a clear statistical hint towards the identification of quarry blasts, but it does not help to discriminate distinct events. The graph suggests that the above-average seismic activity during day time is caused by quarry blasts, but it is not possible to reach a definite decision for each single event (Fig. 2, Table 2 in the Appendix).

4.2 Amplitude ratio A_s/A_p versus $\log(A_s)$

This method compares the amplitude ratio of maximum S to P wave to the logarithm of peak amplitude of S wave in time domain (Wüster 1993; Baumgardt and Young 1990). Although this method is quick and easy, it is not completely reliable.

Discriminant analysis is a classification method that assumes different classes to generate data based on different Gaussian distributions. To create a classifier, the fitting function estimates the parameters of a Gaussian distribution for each class. To predict the classes of new data, the created classifier finds the class with the smallest misclassification. Here in this study, linear and quadratic discriminant analyses were applied (Krzanowski 1988; Seber 1984; MATLAB Release 2011). Linear discriminant function (LDF) analysis (Eq. 1) estimates one covariance matrix for all classes, whereas the quadratic discriminant function (QDF) analysis (Eq. 2) estimates one covariance matrix for each class (Kuyuk et al. 2014).

$$F_{\mathrm{LDF}} = K + L(1)*x + L(2)*y \tag{1}$$

$$F_{\mathrm{QDF}} = K1 + [x\ \ y]*L1 + \sum\{([x\quad y]*Q1)*[x\quad y]\} \tag{2}$$

where K is a constant term of the boundary equation, Ls are linear coefficients of the boundary equation, and Q is quadratic coefficient matrix of the boundary equation. Their indices are the coefficients of the linear or quadratic boundaries between the classes.

The events were determined in the time domain using amplitude ratio method. Figure 3a, b, shows the As/Ap versus log(As) distribution. Among the scattering variables, the discrimination line and curve were drawn by LDF and QDF algorithms. The discrimination procedure was used to define a linear and quadratic combination of quantitative variables that characterized the differences between the groups.

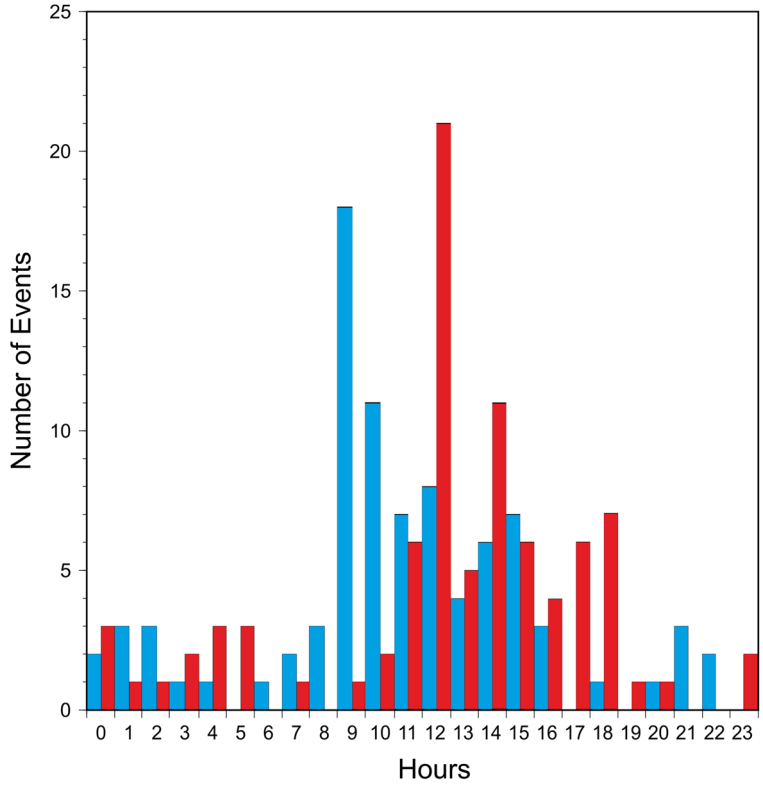

Fig. 2 Time of day frequency distributions of 87 seismic events. The blue and red bins depict GMT and local time, respectively (corrected for summer and winter time periods)

Using the LDF algorithm and comparing with the gold standard, 21 earthquakes and 56 quarry blasts were clearly discriminated, totally ten events were misclassified. Performing the QDF algorithm, 21 earthquakes and 55 quarry blasts were determined, whereas 11 events could not be classified (Table 1, Table 2 in the Appendix).

Calculated parameters for As/Ap–log(As) methods with linear and quadratic forms are Eqs. 3 and 4

$$F_{\mathrm{LDF}} = 8.9203 + (-1.3924)*\log \mathrm{A_s} + (-2.6261)*\mathrm{A_s}/\mathrm{A_p} \tag{3}$$

$$F_{\mathrm{QDF}} = (-10.0562) + [\log \mathrm{A_s} \quad \mathrm{A_s}/\mathrm{A_p}]*\begin{bmatrix} 6.3013 \\ 7.4494 \end{bmatrix} + \sum\left\{\left([\log \mathrm{A_s} \quad \mathrm{A_s}/\mathrm{A_p}]*\begin{bmatrix} -0.8487 & -0.5677 \\ -0.5677 & -3.6037 \end{bmatrix}\right)*[\log \mathrm{A_s} \quad \mathrm{A_s}/\mathrm{A_p}]\right\} \tag{4}$$

4.3 Complexity versus spectral ratio

In this method, first, the seismogram is divided into two time windows (t_0–t_1, t_1–t_2) and the spectral ratio of integrated powers $s^2(t)$ of each part is then calculated. It is called complexity (C) and depends on the epicentral distance. Second, ratio of integrated spectral amplitudes a(f) in the different frequency bands (h_1–h_2, l_1–l_2, high and low frequency band, respectively) is calculated from the waveform of an event. It is called spectral ratio (Sr) and depends on the frequency content of an event. C and Sr can be written in Eq. 5 and Eq. 6, respectively (Arai and Yosida 2004; Gitterman and Shapira 1993).

$$\mathrm{C} = \int_{t_1}^{t_2} s^2(t)dt \Big/ \int_{t_0}^{t_1} s^2(t)dt \tag{5}$$

$$\mathrm{Sr} = \int_{h_1}^{h_2} a(f)df \Big/ \int_{l_1}^{l_2} a(f)df \tag{6}$$

Because epicentral distances differ, distance grouping of the events is important in order not to lose the phases within the selected windows. In conjunction with this, the frequency contents differ for each event, too.

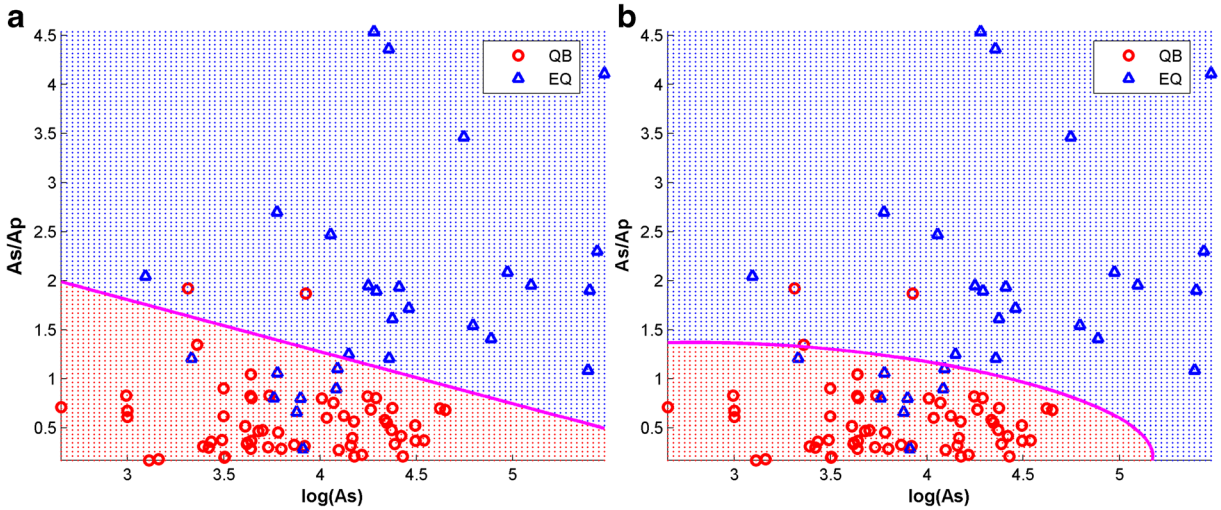

Fig. 3 Amplitude peak ratio of S to P wave (A_s/A_p) versus logarithm of amplitude peak of S wave ($\log(A_s)$) of the vertical component of the velocity seismogram for station KRSK. The classification was performed with **a** linear discriminant function analysis and **b** quadratic discriminant function analysis. Blue triangles and red circles depict earthquakes (EQ) and quarry blasts (QB), respectively. The pink line and curve indicate the discrimination of earthquake and quarry blast using LDF and QDF algorithms

That is why, in this study, the seismograms were divided into two different time windows and frequency bands for station KRSK. Thus, 59 and 28 records at 0–13-km and 13–23-km epicentral distances were analyzed, respectively. At short distances, the time windows were selected as t_0, P wave onset time; t_1, 1.5 s; and t_2, 3 s; otherwise, in long distances, t_0 is not changed, but t_1, 2.5 s, and t_2, 5 s, were chosen. The frequency bands were determined as h_1, 5 Hz; h_2, 10 Hz; l_1, 1 Hz; and l_2, 5 Hz, for all seismograms. Two statistical approaches (LDF and QDF analyses as mentioned in the "Amplitude ratio A_s/A_p versus $\log(A_s)$" section) were used for classification of natural and artificial events.

The C versus Sr distributions are shown for 0–13 km of epicentral distances in Fig. 4a, b, and for 13–23 km in Fig. 5a, b. The discrimination line and curve were derived by LDF and QDF algorithms due to sprinkled variables.

When compared to the gold standard, ten earthquakes and 43 quarry blasts were confirmed and six events were misclassified by using both LDF and QDF algorithms for 0–13-km epicenter distance events. On

Table 1 Classification results of As/Ap–log(As) and complexity-spectral ratio using LDF and QDF algorithms on Figs. 3a, b, 4a, b, and Fig. 5a, b; coda wave decay rate and power spectrum density method analysis (Figs. 7, 8) of all events based on the "gold standard"

Discrimination method	Statistical approach	Count				Success percentage (%)		
		EQ	QB	Misclassified EQ	Misclassified QB	EQ	QB	General
As/Ap–log(As)	LDF	21	56	8	2	72.4	96.5	88.5
	QDF	21	55	8	3	72.4	94.8	87.4
C–Sr	LDF ($0 < D \leq 13$ km)	11	42	4	2	73.3	95.5	89.8
	QDF ($13 < D \leq 23$ km)	11	42	4	2	73.3	95.5	89.8
	LDF ($0 < D \leq 13$ km)	11	13	3	1	78.6	92.9	85.7
	QDF ($13 < D \leq 23$ km)	11	14	3	0	78.6	100	89.3
Q_c	–	26	54	3	4	89.7	93.1	91.9
PSD	–	29	52	0	6	100	89.7	93.1

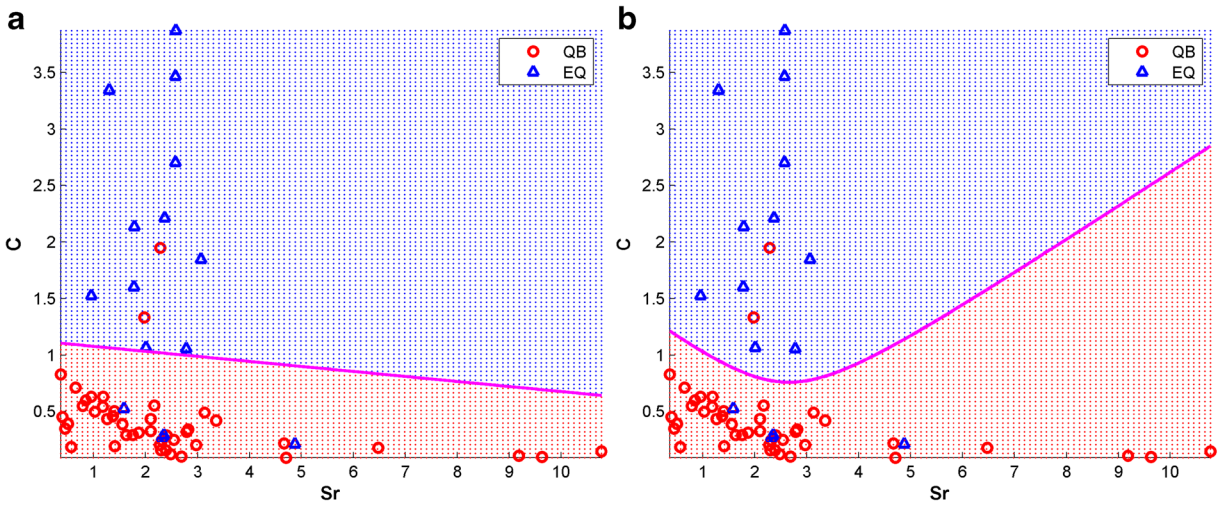

Fig. 4 Plot of complexity (**C**) versus spectral ratio (Sr) of the vertical component of the velocity seismograms of KRSK for events with 0–13 km of epicentral distance. The classification was performed with **a** linear discriminant function and **b** quadratic discriminant function analysis. Blue triangles and red circles depict earthquakes (EQ) and quarry blasts (QB), respectively. The pink line and curve indicate the discrimination of earthquake and quarry blast using LDF and QDF algorithms

the other hand for the epicentral distance range of 13–23 km, 11 earthquakes and 13 quarry blasts were correctly identified with the LDF algorithm, while four events could not be discriminated. Using QDF algorithm for the same distance range, 11 earthquakes and 14 quarry blasts were correctly determined, while three events were not (Table 1, Table 2 in the Appendix).

Calculated parameters of the C versus Sr analyses for the events between 0–13-km and 13–23-km epicenter distances with linear and quadratic forms are shown below with Eqs. 7–10:

$$0\text{–}13\ \text{km};\ F_{\text{LDF}} = 3.5546 + (-0.1407)*\text{Sr} + (-3.1691)*\text{C} \tag{7}$$

$$0\text{–}13\ \text{km};\ F_{\text{QDF}} = 3.6024 + [\text{Sr}\quad \text{C}]*\begin{bmatrix}-2.5060\\ 3.5140\end{bmatrix} + \Sigma\left\{\left([\text{Sr}\quad \text{C}]*\begin{bmatrix}0.5040 & -0.1131\\ -0.1131 & -4.7056\end{bmatrix}\right)*[\text{Sr}\quad \text{C}]\right\} \tag{8}$$

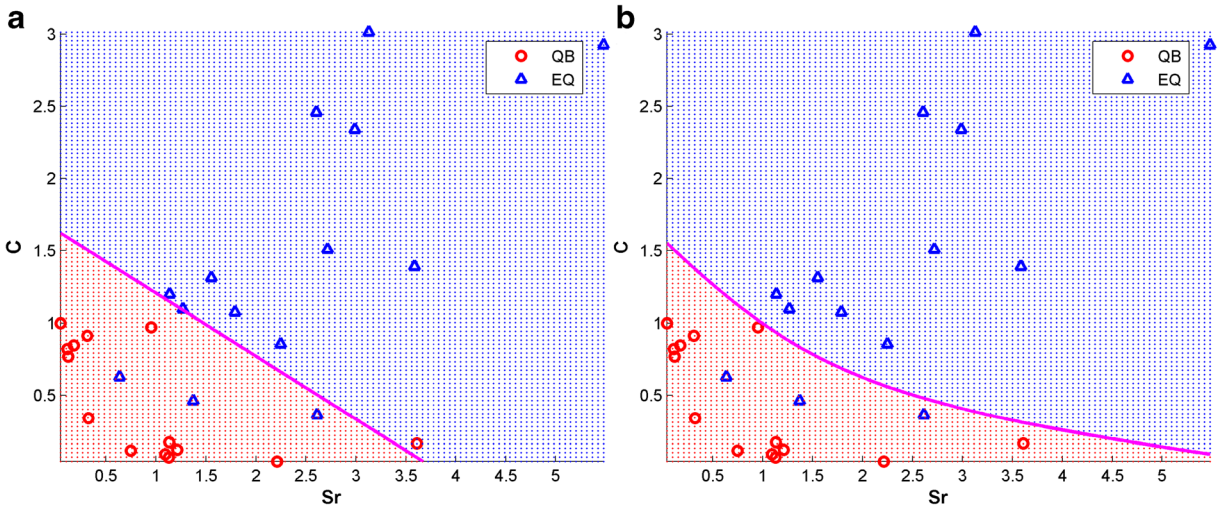

Fig. 5 Plot of complexity (C) versus spectral ratio (Sr) of the vertical component of the velocity seismogram of KRSK for 13–23 km epicentral distances. For details see Fig. 4

$$13\text{–}23\ \text{km};\ F_{\mathrm{LDF}} = 2.8097 + (-0.7458)\text{*Sr} + (-1.7076)\text{*C} \tag{9}$$

$$13\text{–}23\ \text{km};\ F_{\mathrm{QDF}} = (-0.1773) + [\mathrm{Sr}\quad \mathrm{C}]\text{*}\begin{bmatrix}1.6954\\6.3432\end{bmatrix} + \Sigma\left\{\left([\mathrm{Sr}\quad \mathrm{C}]\text{*}\begin{bmatrix}-0.2608 & -1.8429\\-1.8429 & -3.9308\end{bmatrix}\right)\text{*}[\mathrm{Sr}\quad \mathrm{C}]\right\} \tag{10}$$

4.4 Coda wave decay rate versus frequency

The solution for a damped harmonic oscillator incorporates damping described through the dimensionless quality factor (Q). It is used to describe the decay of an oscillator or the physical properties of a system that causes a disturbance to attenuate (Stein and Wysession 2003). In other words, it can be define as the ratio of energy loss per cycle to total energy. Coda waves, also known as the wave train of S waves, from small local earthquakes, are interpreted as backscattered waves from numerous heterogeneities distributed uniformly in the earth's crust (Aki and Chouet 1975). The attenuation characteristic obtained from coda waves defines a coda wave quality factor (Q_c). The amplitude of coda waves entirely depends on distance, time, and frequency. Equation 11 indicates the frequency dependency of Q_c.

$$Q_c(f) = Q_o\left(\frac{f}{f_o}\right)^n \tag{11}$$

In this equation, f_o is the reference frequency; Q_o is the Q_c at 1 Hz and n indicates the frequency dependence. The different frequency contents of earthquakes and quarry blasts are linked to different source types and thus can be used for event discrimination (Su et al. 1991; Hartse et al. 1995). Quarry blasts have simpler spectra than earthquakes. The coda decay rate, Q_c, is significantly lower for quarry blasts than for earthquakes (Kiszely 2005).

The determined coda wave envelope is important for calculating Q_c. At lower frequency bands and shorter coda wave envelopes, the difference of coda wave attenuation between earthquakes and quarry blasts can be easily recognized. Otherwise, at increasing frequency bands and lengthened time windows, the difference cannot be observed, because the waves rapidly decay at shallow depths. Generally, attenuation decreases with depth. Thus, it can be easily understood that attenuation is very strong for quarry blasts which are located at shallow depths. This technique aims to detect the decay rate from the slopes.

As a fourth discrimination method, the signals were evaluated by coda wave decay rate. The absorption of energy should be different for earthquakes and quarry blasts, although a medium has a filter effect that leads to attenuation. It is known that earthquakes have wide frequency bands; while quarry blasts have limited frequencies, because explosions have generally frequency-controlled sources (Kiszely 2005). In this method, 10 to 35 s with 5-s interval coda wave envelopes were chosen and 1.5, 3, 6, 9, and 12-Hz center frequency bands were performed for each time window. All seismograms were digitally bandpass-filtered considering the constant bandwidth filtering, to get a comparable amount of energy into each band. The events have such a close epicenter distances to station KRSK that the coda window was selected to start at 1.5-s travel time from the origin. Figure 6 shows an example of the determined coda window for calculating attenuation rate at station KRSK. The CODAQ subroutine integrated in SEISAN software was used to calculate the quality factor (Havskov and Ottemoller 1999).

Hartse et al. (1995) analyzed the source factor difference in Nevada using coda waves. This method distinguishes between different events while concentrating on smaller magnitudes. Identifying event types with an attenuation rate on various frequencies is effective for this method. Kizsely (2005) used a Q_c in Vértes Mountains, Hungary. At 6-Hz and 10-Hz corner frequencies, the difference between natural and artificial events is most prominent. Aki (1995) has successfully discriminated quarry blasts and earthquakes at local distance by using coda Q method with testing lower and higher frequency bands.

In this study, up to M = 3.0 duration magnitudes were used for discrimination and Q_c can be easily seen at all corner frequencies. If Q_c^{-1} values of increasing coda wave window length decrease more rapidly (i.e., higher slope), the event should be a quarry blast; otherwise, for earthquakes, the slope is much lower. The classification of the events has been done by visual inspection of the slopes. Figure 7 demonstrates the results of the attenuation rate

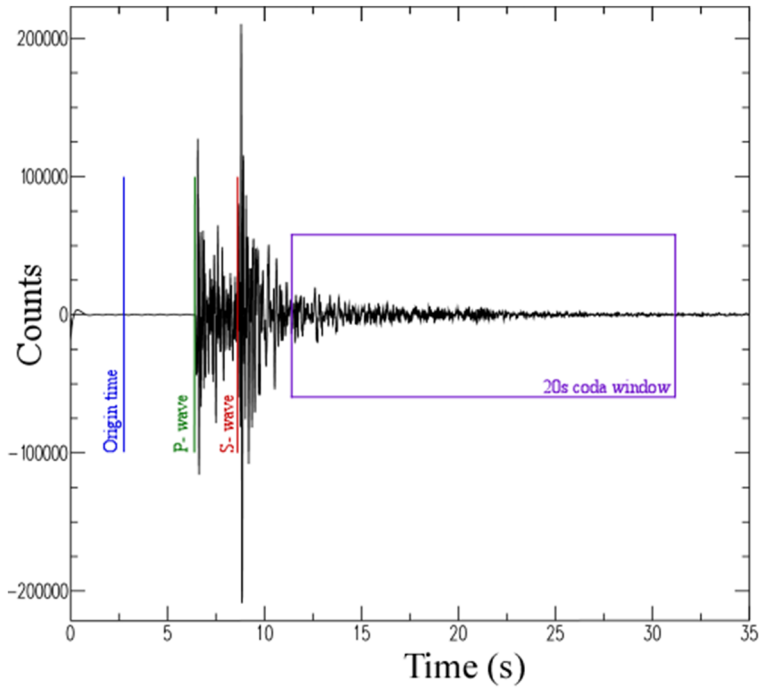

Fig. 6 Example of the 20-s coda window on the vertical component at station KRSK. Event occurred on 22/07/2014 04:18:02.9 GMT ($M_d = 2.5$)

at different frequencies of earthquakes and quarry blasts, separately. Focusing on the decay rate, events could be discriminated in an easier and more decisive way than with previous methods; yet, the quarry blasts were still indistinguishable after a certain coda wave window length. For these cases, the irregular scattered values prevented the correct identification of earthquakes and quarry blasts. With respect to coda wave decay rate method, 80 events were identified and seven events were not classified in compliance with the gold standard (Table 1, Table 2 in the Appendix). The success rate of this method was calculated as 91.9%.

4.5 Power spectrum density versus frequency

Power spectrum density (PSD) is known as the strength of the energy versus frequency, which may show strong or weak frequency variations in the whole signal or in a selected part of it. Comparing the energies of all events, the power spectra of quarry blasts decrease more sharply with increasing frequency than those of earthquakes showing a more stable pattern (Su et al. 1991). Moreover, the Po(ω) value at 1 Hz (beginning) and the same value at 10 Hz (end) are important for classification. Artificial events have lower end spectra with regard to their beginning. Allmann et al. (2008) compared the P wave power spectra of different events for Southern California. They obtained a constant stress-drop model for earthquakes; otherwise, the model curve has a steeper trend for quarry blasts. Ataeva et al. (2017) analyzed the P and S wave displacement spectra ratio of natural and artificial quakes. It can be pointed out that the difference in the ratios can be effective for discrimination. Aki (1995) noted that the power spectra of quarry blasts decrease sharper with increasing frequencies than those of earthquakes. Hence, the comparison of PSD shows remarkable difference between earthquakes and explosions.

In this study, PSD was calculated by GEOPSY software (Wathelet 2005) within 1 to 10-Hz frequency band between the beginning and the final point of the signal for station KRSK. The discrimination was done by visual comparison of the power spectral values at 1 Hz (beginning) and 10 Hz (end). According to the distribution of power spectra versus frequency graphics, earthquakes and quarry blasts were separated using the frequency contents as shown in Fig. 8. Considering the PSD analysis for 87 seismic events, 35 earthquakes and 52 quarry blasts were clearly discriminated from each other with the accuracy of 93.1% (Table 1, Table 2 in the Appendix).

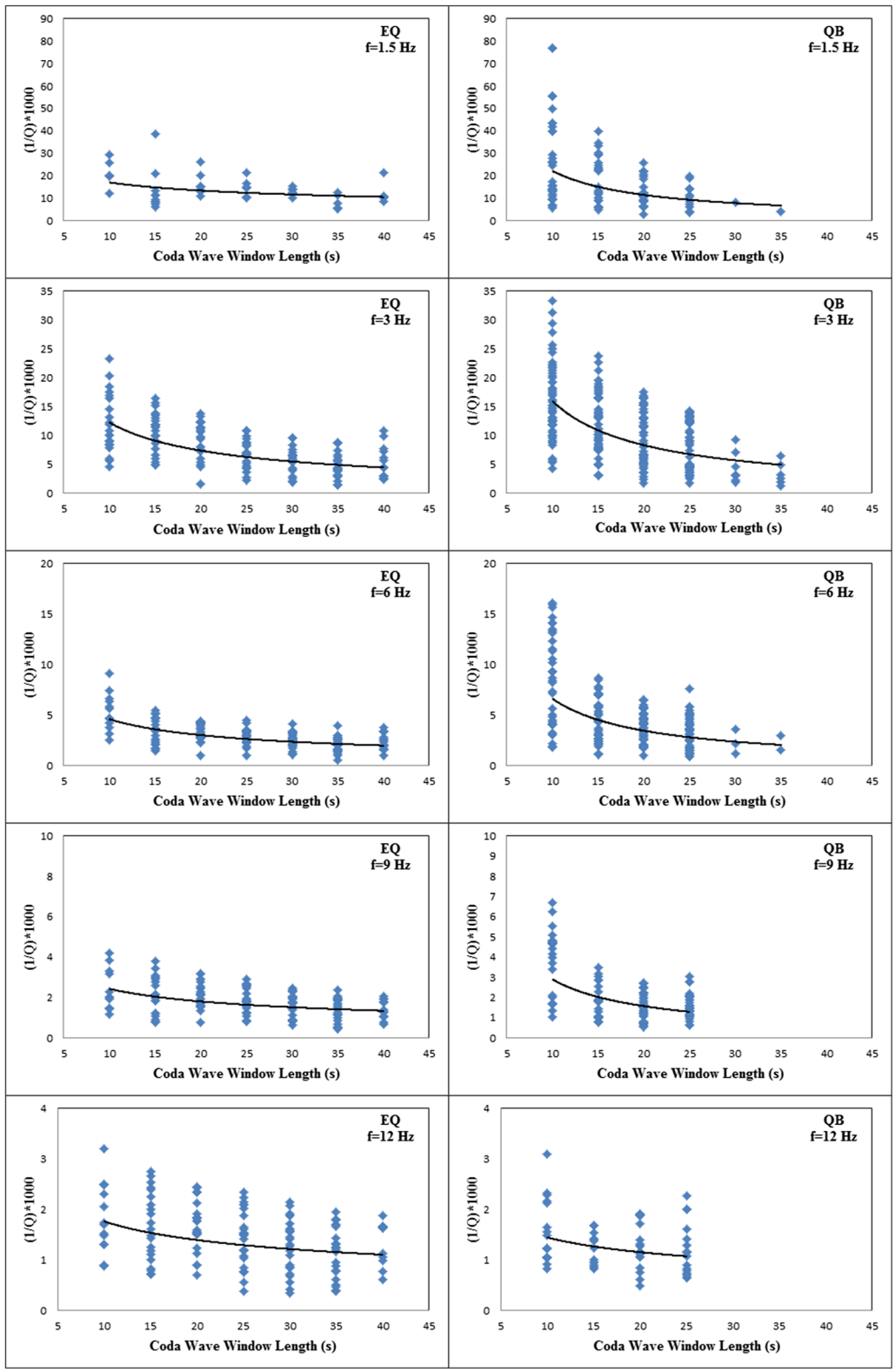

Fig. 7 Coda wave decay rate (Q_c^{-1}) versus coda wave window length obtained from all seismic events. The boxes show the attenuation rate for different frequency ranges. EQ, earthquakes; QB, quarry blasts; f, center frequency

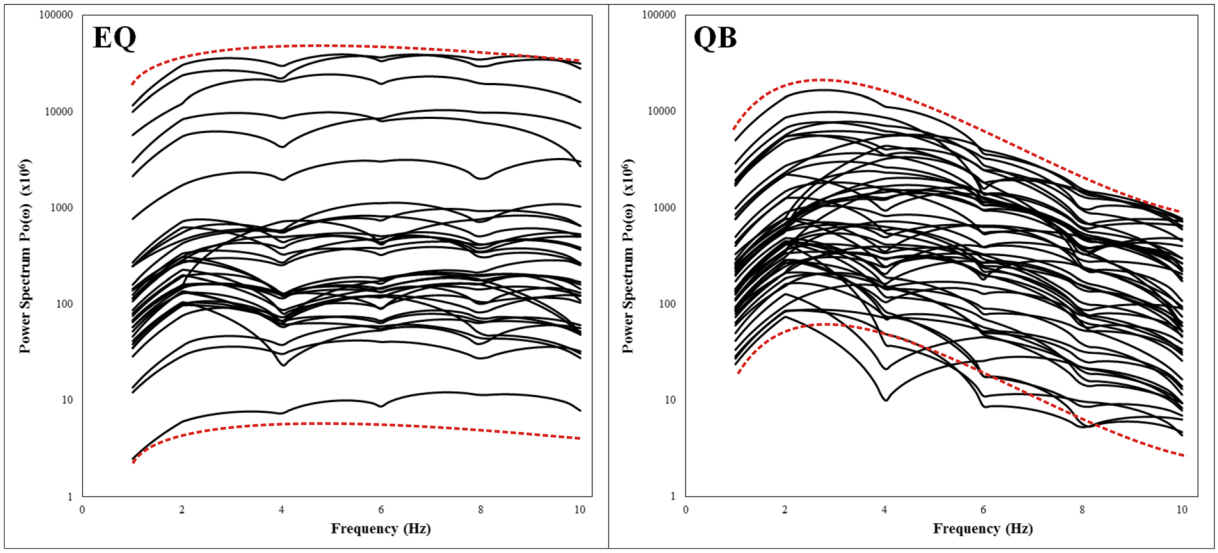

Fig. 8 Power spectrum density versus frequency obtained at station KRSK within 1 to 10-Hz frequency range. The dashed red lines indicate the upper and lower PSD changes of earthquakes and quarry blasts. EQ, earthquakes; QB, quarry blasts

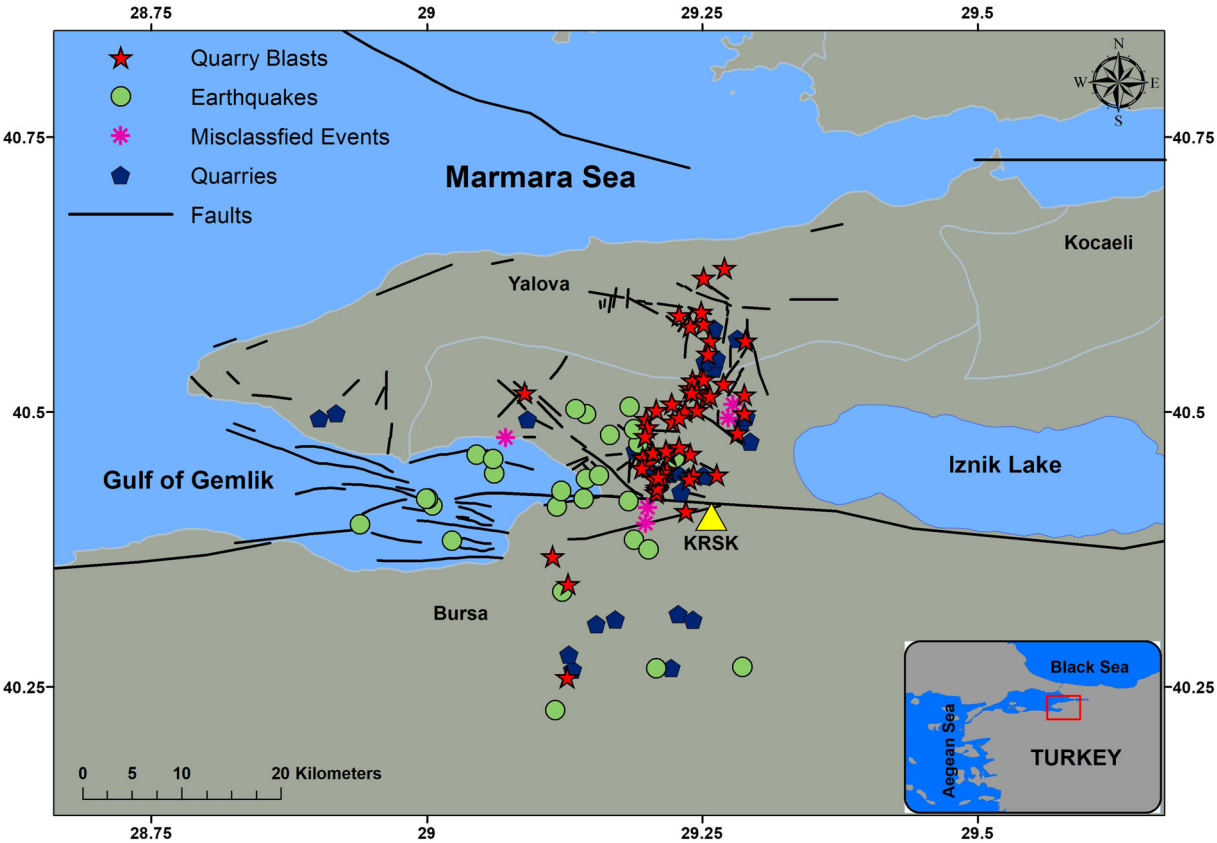

Fig. 9 Location of the identified earthquakes (green circles), quarry blasts (red stars), and misclassified events (pink asterisks) through the final decision (with accuracy 97.7%). The seismic station KRSK is the yellow triangle and blue pentagons depict quarries

4.6 Comparison of different techniques

Table 1 provides a comparison of the performance of different discrimination techniques with respect to the "gold standard," the PSD technique standing with the highest success rate (93.1% in overall). To reach a final decision on the classification of each event, the results of all methods were evaluated and a decision was made when at least three of five methods yielded the same event type. However, the day time of the event helped to differentiate 21 earthquakes; therefore, for the remaining 66 events, we have results of four methods only. In fact, the five misclassified cases are those for which we cannot make a decision as two of the methods discriminate them as earthquake while the remaining two as blasts. The linear and quadratic forms of the two methods could also be used to make final decision; but, they are not helpful in the present cases, as both forms give the same results. From the 87 events, 27 earthquakes and 55 quarry blasts could be discriminated, while five events were misclassified (Table 2 in the Appendix). This final decision was compared with the "gold standard" and the accuracy is calculated as 94.2%. Epicenters of the earthquakes and quarry blasts according to the final decision are plotted in Fig. 9.

5 Conclusion

In this study, 87 events were classified with manual investigation and five different methods including two kinds of statistical approaches. All events were first classified manually yielding the so-called "gold standard"; then other methods were compared to it. A sharp increase of events at 11:00 local time indicates quarry blast activities, but does not allow the discrimination of natural and artificial events. The amplitude peak ratio method could not provide a clear event classification. Similarly, the C versus Sr method, where classification lines and curves were determined by LDF and QDF for two different distance intervals (0–13 km, 13–23 km), could not clearly discriminate the events. In both methods, the use of the linear and quadratic forms did not provide any significant change in the resulting discrimination. The average slopes of the Q_c with increasing window lengths could differentiate the events except 12-Hz central frequency and narrow coda wave window lengths. With respect to the PSD technique, earthquakes have preserved their energies at variable frequencies, whereas quarry blasts have lost more energy with increasing frequencies. Among with 87 seismic events at the first 7 months of 2014, 35 earthquakes and 52 quarry blasts were classified with the accuracy of 93.1% with respect to the "gold standard." Thus, the frequency domain PSD method could provide more reliable results than the others. For the final decision, all methods were compared to each other and the solutions were combined (Table 2 in the Appendix). The events were classified with five methods including two statistical approaches. Hence, 27 earthquakes and 55 quarry blasts were identified using all different methods and five events were misclassified obtaining a success rate as 94.2%.

The discriminant functions that are evaluated for this study are special for this region and used data sets. The crustal structure, the characteristics of the quarry blasts, and different located events may generally change the parameters of these functions. Therefore, the LDF and QDF can only be useful for future studies in and around the Armutlu Peninsula. Nevertheless, a multi-method application is recommended for areas with similar problems to distinguish better between tectonic and anthropogenic seismic activities.

The discrimination of natural-artificial events is important for tectonically active, geologically complex regions with frequent mine activities. The event classification has to be effective and is crucial for seismological and seismicity studies. Recently, the infrastructure on the Armutlu Peninsula is developing rapidly, with planned constructions of new factories, highways, tunnels, bridges, etc., and it is one of the seismically active regions that should be carefully monitored. Therefore, detailed analyses and interpretations can provide and contribute the basic information about the seismic activity of the peninsula.

Acknowledgements We would like to thank Mariano Garcia-Fernandez, PhD. (associate editor), and anonymous reviewers for their helpful comments that improved the manuscript. Many thanks to Kocaeli University Earth and Space Sciences Research Center (KOU-ESSRC) and GFZ (German Research Centre for Geosciences) for ARNET operation and data sharing.

Appendix

Table 2 Classification of all events with different methods and final decision

No.	Event date and origin time (GMT)	Epicenter coordinates		Manual	Discrimination methods							Final
					Time	As/Ap–log(As)		C–Sr		Coda	PSD	
		Latitude (°N)	Longitude (°E)			Statistical approaches						
						LDF	QDF	LDF	QDF			
1	29.07.2014 22:38:02.9	40.461	29.045	EQ	EQ	QB	QB	EQ	EQ	EQ	EQ	EQ
2	26.07.2014 09:08:00.8	40.516	29.288	QB		QB	QB	QB	QB	QB	QB	QB
3	22.07.2014 15:38:34.8	40.578	29.239	QB		QB	QB	QB	QB	QB	QB	QB
4	22.07.2014 04:18:03.7	40.341	29.129	EQ	EQ	EQ	EQ	EQ	EQ	QB	EQ	EQ
5	12.07.2014 08:13:59.3	40.459	29.196	QB		QB	QB	QB	QB	QB	QB	QB
6	05.07.2014 07:35:26.1	40.502	29.132	EQ	EQ	QB	QB	QB	QB	EQ	EQ	EQ
7	04.07.2014 12:34:14.0	40.444	29.061	EQ		EQ	EQ	EQ	EQ	EQ	EQ	EQ
8	03.07.2014 09:19:10.4	40.348	29.135	QB		QB	QB	QB	QB	QB	QB	QB
9	01.07.2014 12:02:15.3	40.369	29.114	QB		QB	QB	QB	QB	QB	QB	QB
10	25.06.2014 21:57:19.1	40.439	29.144	EQ	EQ	QB	QB	EQ	EQ	QB	EQ	EQ
11	21.06.2014 09:03:11.2	40.494	29.199	QB		QB	QB	QB	QB	QB	QB	QB
12	21.06.2014 08:07:59.5	40.501	29.234	QB		QB	QB	QB	QB	QB	QB	QB
13	16.06.2014 02:34:59.4	40.383	29.023	EQ	EQ	EQ	EQ	EQ	EQ	EQ	EQ	EQ
14	14.06.2014 14:03:09.2	40.508	29.222	QB		QB	QB	QB	QB	QB	EQ	QB
15	14.06.2014 09:24:56.4	40.491	29.223	QB		QB	QB	QB	QB	QB	QB	QB
16	12.06.2014 09:36:24.7	40.588	29.229	QB		QB	QB	QB	QB	QB	QB	QB
17	12.06.2014 09:17:00.0	40.462	29.239	QB		QB	QB	QB	QB	QB	QB	QB
18	11.06.2014 11:19:22.0	40.479	29.069	QB		QB	QB	QB	QB	QB	QB	QB
19	06.06.2014 11:30:50.1	40.401	29.199	EQ		EQ	EQ	QB	QB	QB	EQ	MC
20	06.06.2014 10:46:42.9	40.384	29.188	EQ		EQ	EQ	EQ	EQ	EQ	EQ	EQ
21	04.06.2014 01:37:01.5	40.267	29.208	EQ	EQ	EQ	EQ	EQ	EQ	EQ	EQ	EQ
22	03.06.2014 09:20:52.9	40.454	29.201	QB		QB	QB	QB	QB	QB	EQ	QB
23	03.06.2014 09:13:54.7	40.429	29.209	QB		QB	QB	QB	QB	QB	QB	QB
24	03.06.2014	40.498	29.144	EQ	EQ	EQ	EQ	EQ	EQ	EQ	EQ	EQ

Table 2 (continued)

No.	Event date and origin time (GMT)	Epicenter coordinates		Manual	Discrimination methods							Final
					Time	As/Ap–log(As)		C–Sr		Coda	PSD	
		Latitude (°N)	Longitude (°E)			Statistical approaches						
						LDF	QDF	LDF	QDF			
25	00:30:00.5 30.05.2014 12:01:15.3	40.505	29.284	QB		QB	QB	EQ	EQ	QB	EQ	MC
26	29.05.2014 13:43:59.7	40.522	29.239	QB		QB	QB	QB	QB	QB	QB	QB
27	28.05.2014 11:24:40.8	40.449	29.195	QB		QB	QB	QB	QB	QB	QB	QB
28	25.05.2014 15:51:44.0	40.580	29.251	QB		QB	QB	QB	QB	QB	QB	QB
29	25.05.2014 10:29:28.4	40.531	29.249	QB		QB	QB	QB	QB	QB	QB	QB
30	23.05.2014 11:13:14.7	40.439	29.207	QB		QB	QB	QB	QB	QB	QB	QB
31	17.05.2014 12:03:36.4	40.529	29.241	QB		QB	QB	EQ	QB	QB	QB	QB
32	17.05.2014 11:58:28.1	40.530	29.251	QB		QB	QB	QB	QB	EQ	QB	QB
33	16.05.2014 15:17:40.2	40.414	29.118	EQ		EQ	EQ	EQ	EQ	EQ	EQ	EQ
34	14.05.2014 09:21:31.7	40.478	29.199	QB		QB	QB	QB	QB	QB	QB	QB
35	12.05.2014 11:18:29.6	40.419	29.183	EQ		EQ	EQ	QB	QB	EQ	EQ	EQ
36	12.05.2014 09:36:34.8	40.443	29.263	QB		QB	QB	QB	QB	QB	QB	QB
37	10.05.2014 15:15:38.4	40.565	29.289	QB		QB	QB	QB	QB	QB	QB	QB
38	09.05.2014 21:41:49.5	40.505	29.184	EQ	EQ	EQ	EQ	EQ	EQ	EQ	EQ	EQ
39	09.05.2014 10:57:12.3	40.463	29.205	QB		QB	QB	QB	QB	QB	QB	QB
40	09.05.2014 02:33:28.7	40.457	29.060	EQ	EQ	EQ	EQ	EQ	EQ	EQ	EQ	EQ
41	07.05.2014 01:57:51.2	40.428	29.122	EQ	EQ	EQ	EQ	EQ	EQ	EQ	EQ	EQ
42	06.05.2014 16:46:44.2	40.231	29.121	EQ	EQ	QB	QB	QB	QB	EQ	EQ	EQ
43	06.05.2014 14:09:30.1	40.495	29.229	EQ		QB	QB	QB	QB	EQ	EQ	MC
44	03.05.2014 09:03:01.4	40.502	29.245	QB		QB	QB	QB	QB	QB	QB	QB
45	03.05.2014 09:02:16.6	40.427	29.208	QB		QB	QB	QB	QB	QB	QB	QB
46	02.05.2014 15:44:23.4	40.565	29.257	QB		QB	QB	QB	QB	QB	QB	QB
47	01.05.2014 14:03:40.0	40.431	29.209	QB		QB	QB	QB	QB	QB	QB	QB
48	01.05.2014 09:09:46.2	40.486	29.200	QB		QB	QB	QB	QB	QB	QB	QB
49	28.04.2014	40.414	29.201	QB		EQ	EQ	EQ	EQ	QB	QB	MC

Table 2 (continued)

No.	Event date and origin time (GMT)	Epicenter coordinates		Manual	Discrimination methods							Final
					Time	As/Ap–log(As)		C–Sr		Coda	PSD	
		Latitude (°N)	Longitude (°E)			Statistical approaches						
						LDF	QDF	LDF	QDF			
50	10:34:38.8 25.04.2014 10:26:49.5	40.447	29.218	QB		QB	QB	QB	QB	QB	QB	QB
51	25.04.2014 07:36:38.9	40.517	29.092	QB	EQ	QB	QB	QB	QB	EQ	QB	QB
52	24.04.2014 08:58:37.5	40.513	29.253	QB	EQ	QB	QB	QB	QB	QB	QB	QB
53	24.04.2014 06:13:11.6	40.553	29.255	QB	EQ	QB	QB	QB	QB	QB	QB	QB
54	13.04.2014 20:53:48.5	40.415	29.005	EQ	EQ	QB	QB	EQ	EQ	EQ	EQ	EQ
55	12.04.2014 13:49:01.1	40.259	29.127	QB		QB	EQ	QB	QB	QB	QB	QB
56	08.04.2014 11:52:18.7	40.481	29.282	QB		QB	QB	QB	QB	QB	QB	QB
57	08.04.2014 09:15:05.1	40.461	29.220	QB		QB	QB	QB	QB	QB	QB	QB
58	02.04.2014 09:34:48.4	40.421	29.001	EQ		EQ	EQ	EQ	EQ	EQ	EQ	EQ
59	30.03.2014 14:24:04.6	40.468	29.229	QB		QB	QB	QB	QB	QB	EQ	QB
60	24.03.2014 16:42:04.0	40.631	29.270	QB		QB	QB	QB	QB	QB	QB	QB
61	23.03.2014 01:57:17.7	40.479	29.166	EQ	EQ	EQ	EQ	EQ	EQ	EQ	EQ	EQ
62	16.03.2014 12:50:32.0	40.445	29.214	QB		QB	QB	QB	QB	QB	QB	QB
63	11.03.2014 10:14:03.8	40.375	29.201	EQ		EQ	EQ	QB	QB	EQ	EQ	EQ
64	20.02.2014 12:14:54.4	40.443	29.242	QB		QB	QB	QB	QB	QB	QB	QB
65	20.02.2014 09:54:37.2	40.398	28.939	EQ		QB	QB	EQ	EQ	EQ	EQ	EQ
66	14.02.2014 10:19:22.2	40.502	29.208	QB		QB	QB	QB	QB	QB	QB	QB
67	11.02.2014 10:58:16.1	40.519	29.245	QB		QB	QB	QB	QB	EQ	QB	QB
68	08.02.2014 14:59:14.6	40.622	29.251	QB		EQ	EQ	QB	QB	QB	QB	QB
69	07.02.2014 12:04:24.0	40.526	29.269	QB		QB	QB	QB	QB	QB	QB	QB
70	05.02.2014 16:04:55.1	40.591	29.249	QB		QB	QB	QB	QB	QB	QB	QB
71	05.02.2014 10:09:18.8	40.465	29.217	QB		QB	QB	QB	QB	QB	EQ	QB
72	03.02.2014 10:01:37.0	40.518	29.240	QB		QB	QB	QB	QB	QB	QB	QB
73	02.02.2014 18:37:08.9	40.421	28.999	EQ	EQ	QB	QB	EQ	EQ	EQ	EQ	EQ
74	31.01.2014	40.478	29.198	QB		QB	QB	QB	QB	QB	QB	QB

Table 2 (continued)

No.	Event date and origin time (GMT)	Epicenter coordinates		Manual	Discrimination methods							Final
					Time	As/Ap–log(As)		C–Sr		Coda	PSD	
		Latitude (°N)	Longitude (°E)			Statistical approaches						
						LDF	QDF	LDF	QDF			
75	15:24:51.9 31.01.2014 00:20:02.6	40.471	29.192	EQ		EQ	EQ	EQ	EQ	EQ	EQ	EQ
76	30.01.2014 09:01:55.4	40.515	29.257	QB		QB	QB	QB	QB	EQ	QB	QB
77	28.01.2014 13:11:14.1	40.496	29.271	QB		QB	QB	EQ	EQ	QB	EQ	MC
78	26.01.2014 03:14:04.6	40.484	29.188	EQ	EQ	EQ	EQ	EQ	EQ	EQ	EQ	EQ
79	25.01.2014 14:31:49.7	40.441	29.213	QB		QB	QB	QB	QB	QB	QB	QB
80	23.01.2014 15:53:48.1	40.421	29.142	EQ		EQ	EQ	EQ	EQ	EQ	EQ	EQ
81	22.01.2014 22:41:08.3	40.458	29.225	EQ	EQ	EQ	EQ	EQ	EQ	EQ	EQ	EQ
82	17.01.2014 09:54:04.7	40.441	29.210	QB		QB	QB	QB	QB	QB	QB	QB
83	16.01.2014 02:06:53.3	40.442	29.156	EQ	EQ	EQ	EQ	EQ	EQ	EQ	EQ	EQ
84	11.01.2014 12:59:25.5	40.499	29.288	QB		QB	QB	QB	QB	QB	QB	QB
85	10.01.2014 21:15:47.4	40.268	29.286	EQ	EQ	EQ	EQ	EQ	EQ	EQ	EQ	EQ
86	08.01.2014 10:07:08.9	40.410	29.235	QB		QB	QB	QB	QB	QB	QB	QB
87	07.01.2014 13:36:50.9	40.439	29.238	QB		QB	QB	QB	QB	QB	QB	QB

EQ earthquake, *QB* quarry blast, *MC* misclassified event

References

Akartuna M (1968) The geology of the Armutlu Peninsula. Istanbul University Graduate School of Applied Science Monographies 20:105 (in Turkish)

Aki K (1995) Discriminating underground explosions from earthquakes using seismic coda waves. University of Southern California Los Angeles Center for Earth Sciences

Aki K, Chouet B (1975) Origin of coda waves: source, attenuation, and scattering effects. J Geophys Res 80:3322–3342

Aki K, Richards PG (1980) Quantitative seismology: theory and methods. W. H. Freeman, San Francisco

Allmann BP, Shearer PM, Hauksson E (2008) Spectral discrimination between quarry blasts and earthquakes in Southern California. Bull Seismol Soc Am 98:2073–2079

Arai N, Yosida Y (2004) Discrimination by short-period seismograms. International Institute of Seismology and Earthquake Engineering, Building Research Institute (IISEE). Lecture note, global course, Tsukuba, Japan, p. 10

Armijo R, Meyer B, Hubert A, Barka A (1999) Westwards propagation of the North Anatolian fault into the northern Aegean: timing and kinematics. Geology 27: 267–270

Arrowsmith SJ, Arrowsmith MD, Hedlin MA, Stump B (2006) Discrimination of delay-fired mine blasts in Wyoming using an automatic time-frequency discriminant. Bull Seismol Soc Am 96:2368–2382

Ataeva G, Gitterman Y, Shapira A (2017) The ratio between corner frequencies of source spectra of P- and S-waves—a new discriminant between earthquakes and quarry blasts. J Seismol 21:209–220

Barka A, Akyüz HS, Altunel E, Sunal G, Çakir G, Çakir Z, Dikbaş A, Yerli B, Armijo R, Meyer B, de Chabalier JB, Rockwell T, Dolan JR, Hartleb R, Dawson T, Christofferson S, Tucker A, Fumal T, Langridge R, Stenner H, Lettis W, Bachhuber J, Page W (2002) The surface rupture and slip distribution of the 17 August 1999 İzmit earthquake (M 7.4), North Anatolian fault. Bull Seismol Soc Am 92:43–60

Baumgardt DR, Young GB (1990) Regional seismic waveform discriminants and case-based event identification using regional arrays. Bull Seismol Soc Am 80:1874–1892

Borleanu F, Manea L, Stoicescu D (2016) Lateral variations of Vp/Vs ratios for Romanian upper crust. EGU General Assembly Conference Abstracts 18:17350

Çaka D (2012) Shear-wave splitting analysis in and around Armutlu Peninsula, Ph.D. dissertation, Kocaeli University (in Turkish)

Carr DB, Garbin HD (1998) Discriminating ripple-fired explosions with high-frequency (>16 Hz) data. Bull Seismol Soc Am 88:963–972

Eisenlohr T (1997) The thermal springs of the Armutlu Peninsula (NW Turkey) and their relocationship geology and tectonic. Active Tectonics of Northwestern Anatolia-The Marmara Poly-project, ETH-Zurich, pp 197–228

Gitterman Y, Shapira A (1993) Spectral discrimination of underwater explosions. Isr J Earth Sci 42:37–44

Gitterman Y, Pinsky V, Shapira A (1998) Spectral classification methods in monitoring small local events by the Israel seismic network. J Seismol 2:237–256

Göncüoğlu MC, Erendil M, Tekeli O, Aksay A, Kuşçu I, Urgun BM (1992) Introduction to the geology of Armutlu Peninsula. In: Proc Int Symp on the Geology of the Black Sea Region, pp 26–36

Hartse HE, Phillips WS, Fehler MC, House LS (1995) Single-station spectral discrimination using coda waves. Bull Seismol Soc Am 85:1464–1474

Havskov J, Ottemoller L (1999) SEISAN earthquake analysis software. Seismol Res Lett 70:532–534

Horasan G, Güney AB, Küsmezer A, Bekler F, Öğütçü Z, Musaoğlu N (2009) Contamination of seismicity catalogs by quarry blasts: an example from Istanbul and its vicinity, northwestern Turkey. J Asian Earth Sci 34:90–99

Kekovalı K, Kalafat D, Deniz P (2012) Spectral discrimination between mining blasts and natural earthquakes: application to the vicinity of Tunçbilek mining area, Western Turkey. Int J Phys Sci 7:5339–5352

Kim WY, Aharonian V, Lerner-Lam AL, Richards PG (1997) Discrimination of earthquakes and explosions in southern Russia using regional high-frequency three-component data from the IRIS/JSP Caucasus network. Bull Seismol Soc Am 87:569–588

Kinscher J, Krüger F, Woith H, Lühr BG, Hintersberger E, Irmak TS, Barış Ş (2013) Seismotectonics of the Armutlu peninsula (Marmara Sea, NW Turkey) from geological field observation and regional moment tensor inversion. Tectonophysics 608:980–995

Kiszely M (2005) Annual, monthly, weekly and diurnal distribution of Carpathian (1964-2004) and M>7 earthquakes worldwide (1900-2004) and seeking for the effect of the Moon. Acta Geod Geoph Hung 40:437–454

Koch K, Fäh D (2002) Identification of earthquakes and explosions using amplitude ratios: the Vogtland area revisited. Monitoring the comprehensive nuclear-test-ban treaty: Seismic event discrimination and identification. Birkhäuser, Basel, pp 735–757

Krzanowski WJ (1988) Principles of multivariate analysis: a user's perspective. Clarendon

Kuşçu I, Okamura M, Matsuoka H, Yamamori K, Awata Y, Özalp S (2009) Recognition of active faults and step over geometry in Gemlik bay, Sea of Marmara, NW Turkey. Mar Geol 260:90–101

Kuyuk HS, Yildirim E, Dogan E, Horasan G (2011) An unsupervised learning algorithm: application to the discrimination of seismic events and quarry blasts in the vicinity of Istanbul. Nat Hazards Earth Syst Sci 11:93–100

Kuyuk HS, Yildirim E, Dogan E, Horasan G (2014) Clustering seismic activities using linear and nonlinear discriminant analysis. J Earth Sci 25:140–145

MATLAB Release 2011, The MathWorks, Inc, Natick, Massachusetts, United States

McClusky S, Reilinger R, Mahmoud S, Sari DB, Tealeb A (2003) GPS constraints on Africa (Nubia) and Arabia plate motions. Geophys J Int 155:126–138

Reilinger RE, McClusky SC, Oral MB, King RW, Toksoz MN, Barka AA, Kinik I, Lenk O, Sanli I (1997) Global Positioning System measurements of present-day crustal movements in the Arabia-Africa-Eurasia plate collision zone. J Geophys Res Solid Earth 102:9983–9999

Reilinger R, McClusky S, Vernant P et al (2006) GPS constraints on continental deformation in the Africa-Arabia-Eurasia continental collision zone and implications for the dynamics of plate interactions. J Geophys Res Solid Earth 111:9983–9999

Robertson AH, Ustaömer T (2004) Tectonic evolution of the Intra-Pontide suture zone in the Armutlu Peninsula, NW Turkey. Tectonophysics 381:175–209

Seber GAF (1984) Multivariate observations. John Wiley & Sons, Inc., Hoboken

Sertçelik F, Başer O (2010) Güney Ege Bölgesi'nde yapay ve doğal kaynaklı titreşimlerin ayırt edilmesi (Discrimination of artificial and natural sourced vibrations in the southern Aegean Region). Yerbilimleri 31:233–245 (in Turkish)

Shashidhar D, Mallika K, Rao NP, Satyanarayana HVS, Gupta HK (2014) Detection of quarry blasts in the Koyna-Warna region, western India. Open J Earthquake Res 3:162–169

Stein S, Wysession M (2003) An introduction to seismology, earthquakes, and earth structure. Blackwell Publishing, Oxford

Su F, Aki K, Biswas NN (1991) Discriminating quarry blasts from earthquakes using coda waves. Bull Seismol Soc Am 81:162–178

Tunç B, Çaka D, Irmak TS, Woith H, Tunç S, Barış Ş, Özer MF, Lühr BG, Günther E, Grosser H, Zschau J (2011) The Armutlu Network: an investigation into the seismotectonic setting of Armutlu–Yalova–Gemlik and the surrounding regions. Ann Geophys 54:35–45

Ursino A, Langer H, Scarfi L, Di Grazia G, Gresta S (2001) Discrimination of quarry blasts from tectonic microearthquakes in the Hyblean Plateau (Southeastern Sicily). Ann Geophys 44:703–722

Wathelet M (2005) GEOPSY-geophysical signal database for noise array processing. Software, LGIT, Grenoble

Wiemer S, Baer M (2000) Mapping and removing quarry blast events from seismicity catalogs. Bull Seismol Soc Am 90:525–530

Wüster J (1993) Discrimination of chemical explosions and earthquakes in central Europe—a case study. Bull Seismol Soc Am 83:1184–1212

Yavuz E, Çaka D, Tunç B, Irmak TS, Woith H, Cesca S, Lühr BG, Barış Ş (2015) Earthquake swarm in Armutlu Peninsula, eastern Marmara region, Turkey. EGU General Assembly Conference Abstracts 17:5099

Yıldırım E, Gülbağ A, Horasan G, Doğan E (2011) Discrimination of quarry blasts and earthquakes in the vicinity of Istanbul using soft computing techniques. Comput Geosci 37:1209–1217

Yılmaz Ş, Bayrak Y, Çınar H (2013) Discrimination of earthquakes and quarry blasts in the eastern Black Sea region of Turkey. J Seismol 17:721–734